INTERNATIONAL JOURNAL FOR NUMERICAL METHODS IN FLUIDS
Int. J. Numer. Meth. Fluids 2004; **45**:715–749 (DOI: 10.1002/fld.701)

Two-dimensional dispersion analyses of finite element approximations to the shallow water equations

J. H. Atkinson[1,*,†], J. J. Westerink[1] and R. A. Luettich Jr[2]

[1]*Department of Civil Engineering and Geological Sciences, University of Notre Dame, Notre Dame, IN 46556, U.S.A.*
[2]*Institute of Marine Sciences, University of North Carolina at Chapel Hill, 3431 Arendell Street, Morehead City, NC 28557, U.S.A.*

SUMMARY

Dispersion analysis of discrete solutions to the shallow water equations has been extensively used as a tool to define the relationships between frequency and wave number and to determine if an algorithm leads to a dual wave number response and near $2\Delta x$ oscillations. In this paper, we explore the application of two-dimensional dispersion analysis to cluster based and Galerkin finite element-based discretizations of the primitive shallow water equations and the generalized wave continuity equation (GWCE) reformulation of the harmonic shallow water equations on a number of grid configurations. It is demonstrated that for various algorithms and grid configurations, contradictions exist between the results of one-dimensional and two-dimensional dispersion analysis as a result of subtle changes in the mass matrix. Numerical experiments indicate that the two-dimensional dispersion analysis correctly predicts the existence and onset of near $2\Delta x$ noise in the solution. Copyright © 2004 John Wiley & Sons, Ltd.

KEY WORDS: dispersion analysis; shallow water equations; finite element models

1. INTRODUCTION

Much attention has been devoted in recent decades to developing oscillation-free finite element solutions to the shallow water equations. The earliest finite element schemes for solving the shallow water equations suffered from severe near $2\Delta x$ oscillations or 'wiggles' which often rendered these solutions useless by obscuring the true solution. Approaches to solving this problem have included adding artificial viscosity, using inherently dissipative time stepping schemes [1], using a variety of mixed-order interpolation schemes [2, 3], and employing filters

*Correspondence to: J. H. Atkinson, 3501 Grassland Drive, Norman, OK 73072-2914, U.S.A.
†E-mail: John.H.Atkinson-1@ou.edu

Contract/grant sponsor: U.S. Army Engineer Research and Development Center; contract/grant number: DACW H2-00-C-0006

Published online 19 April 2004

Received 12 July 2002
Revised 20 January 2004

to remove the oscillations from a solution [4]. One of the most widely used finite element solution techniques for solving the shallow water equations is based on reformulating the governing equations into GWCE form prior to discretization [5]. In this approach, oscillation free results are obtained by casting the continuity equation into a form that resembles a wave equation and then applying a standard finite element discretization. All of these developments have been well documented in the literature.

Platzman [6] was the first to realize that spurious modes, or wiggles, result from a discrete dispersion relationship that is folded rather than monotonic like the continuum relationship. A folded dispersion relationship implies that for a given frequency, the discrete model will compute a response at a small wave number (the physical wave) and a large wave number (the wiggle). The undesirable, high wave number response has a wavelength on the order of twice the grid spacing and is therefore referred to as a $2\Delta x$ wave. Therefore, extensive efforts have been made in the search for finite element schemes whose dispersion relationships are monotonic. Foreman [7, 8] and Walters and Carey [2, 9] have thoroughly documented the dispersion relationships of a number of discretization schemes. The advantage of algorithms based upon the GWCE form of the shallow water equations is that they have monotonic dispersion relationships [8, 10].

In the search for solution strategies for the shallow water equations, dispersion analysis must feature prominently since a folded dispersion relationship serves as a proxy for the existence of spurious oscillations. However, in this paper, we demonstrate that a one-dimensional dispersion analysis does not always explain the observed variability of a two-dimensional implementation of a scheme. For instance, it is well known that a one-dimensional linear finite element discretization of the primitive shallow water equations has a folded dispersion relationship and a noisy solution is expected [6]. However, for a two-dimensional discretization of the primitive equations with a linear finite element triangulation we have found that dispersion characteristics depend upon element configuration and wave propagation direction. In addition, we have developed a cluster scheme based upon discretizing the primitive continuity equation with a piecewise constant weighting function. One-dimensional dispersion analysis indicates that this scheme has monotonic behaviour and a dispersion relationship that is identical to that of the one-dimensional wave equation. Nevertheless, numerical experiments on the quarter annular test problem indicate oscillatory behaviour similar to the primitive equation scheme. These examples are in direct contradiction with the one-dimensional dispersion analysis.

In this paper, we exploit two-dimensional dispersion analysis to more accurately discern the dispersion characteristics and behaviour of two-dimensional numerical solutions to the shallow water equations. Two-dimensional analysis was first applied to the shallow water equations by Walters and Carey [2] who examined the dispersion relationship for a node at the junction of six triangles obtained by bisecting rectangles. While they presented the dispersion analysis for only one grid configuration, they stated that their result was indicative of all triangulations. Foreman [11] extended two-dimensional analysis to include the effects of two configurations of six elements. The work of Foreman contradicts the Walters and Carey's result by demonstrating that grid configuration does have an influence on the numerical solution and that the analysis of the bisected quadrilateral configuration is not representative of all configurations. However, both Foreman and Walters and Carey found that the two-dimensional dispersion relationship for any grid configuration could be identically reduced to the one-dimensional analysis by restricting wave propagation to certain directions. Mullen

and Belytschko [12] examined the influence of grid configuration on the dispersion properties of the wave equation formulation and found monotonicity for the wave scheme on all grid configurations. Lynch and Paulsen [13] examined dispersion analysis of the two-dimensional Maxwell equation which resembles the wave continuity equation. However, grid configuration was not examined.

The two-dimensional dispersion analysis presented here is applied to linear triangulations of the primitive and wave equation formulations and a cluster-based discretization of the primitive equations for a variety of grid configurations. We carefully study the dispersion surfaces and their folding characteristics and demonstrate through numerical experiments that two-dimensional dispersion analysis can correctly predict the onset of noisiness of the solutions for various algorithms and grid configurations when one-dimensional analysis fails to do so. Finally, the mass matrix is shown to be fundamental to dispersion properties and it is revealed that subtle differences between the mass matrix in one and two dimensions is responsible for the observed differences in behaviour.

2. GOVERNING EQUATIONS

In this study, attention will be restricted to the linearized, depth averaged, shallow water equations with constant bathymetry. Advective acceleration, Coriolis acceleration, free surface stresses and lateral diffusion and dispersion are neglected, and bottom friction is linearized. Although these restricted equations do not fully describe the physics of real tidal flows, they are satisfactory for investigating the base properties of spatial discretization methods.

The two-dimensional harmonic form of the linearized continuity and momentum equations are

$$(\hat{\mathrm{i}}\omega)\zeta + h\left(\frac{\partial u}{\partial x} + \frac{\partial v}{\partial y}\right) = 0 \tag{1}$$

$$(\hat{\mathrm{i}}\omega + \tau)u + g\frac{\partial \zeta}{\partial x} = 0 \tag{2}$$

$$(\hat{\mathrm{i}}\omega + \tau)v + g\frac{\partial \zeta}{\partial y} = 0 \tag{3}$$

where u and v are the x and y depth-averaged velocities, ζ the surface elevation, h the bathymetric depth, τ the linear bottom friction coefficient, g the gravitational acceleration, and ω the harmonic frequency. Spatial discretizations will be applied to the harmonic form of the governing equations. By casting the equations into harmonic form, the effects of a finite element spatial discretization may be evaluated independently from the choice of time-stepping algorithm. Note that the solutions for the harmonic equations should be the same as the solutions from a consistent time-stepping algorithm as $\Delta t \to 0$.

The dispersion relationship is found through a well-established method [2, 6, 7, 14] of performing a Fourier expansion for the nodal unknowns that appear in the discrete equations. Since the governing equations are linear, the solution may be examined by observing the behaviour of one Fourier mode. This permits the values of the dependent variable at a node

j to be replaced by the Fourier mode

$$\zeta_j = \zeta^o \mathrm{e}^{\hat{\mathrm{i}}k_x x_j + \hat{\mathrm{i}}k_y y_j} \tag{4}$$

$$u_j = u^o \mathrm{e}^{\hat{\mathrm{i}}k_x x_j + \hat{\mathrm{i}}k_y y_j} \tag{5}$$

$$v_j = v^o \mathrm{e}^{\hat{\mathrm{i}}k_x x_j + \hat{\mathrm{i}}k_y y_j} \tag{6}$$

where $\hat{\mathrm{i}} \equiv \sqrt{-1}$ and the two wave numbers k_x and k_y define the direction of propagation at an angle θ given by $\tan(\theta) = k_y/k_x$. The x_j, y_j nodal co-ordinates are expressed in terms of the distance from a reference node, and the result is a square matrix system for the Fourier amplitudes ζ^o, u^o and v^o of the form

$$\begin{bmatrix} P1 & P2 & P3 \\ Q1 & Q2 & 0 \\ R1 & 0 & R3 \end{bmatrix} \begin{Bmatrix} \zeta^o \\ u^o \\ v^o \end{Bmatrix} = \begin{Bmatrix} 0 \\ 0 \\ 0 \end{Bmatrix} \tag{7}$$

For a non-trivial solution to exist, the determinant of the matrix must equal zero, and this constraint yields a dispersion relationship between the two wave numbers k_x and k_y, and the harmonic frequency ω. For the discrete equations, the expressions for $P1$, $P2$, $P3$, $Q1$, $Q2$, $R1$ and $R3$ will be functions of the grid spacing. Since the expressions may be quite complicated, the algebraic manipulations were performed with the Maple and Mathematica sofware packages. The detailed form of the Fourier system matrix may be found in Reference [15] for all of the discretizations presented here.

When this analysis is performed on the continuum equations, the following dispersion relationship is obtained:

$$\omega = \frac{\hat{\mathrm{i}}\tau}{2} \pm \sqrt{gh(k_x^2 + k_y^2) - \left(\frac{\tau}{2}\right)^2} \tag{8}$$

In the non-dimensional variables,

$$\Omega \equiv \frac{\omega L}{\pi\sqrt{gh}} \tag{9}$$

$$K_x \equiv \frac{k_x \Delta x}{\pi} \tag{10}$$

$$K_y \equiv \frac{k_y \Delta y}{\pi} \tag{11}$$

$$T \equiv \frac{\tau}{\sqrt{gh(k_x^2 + k_y^2)}} \tag{12}$$

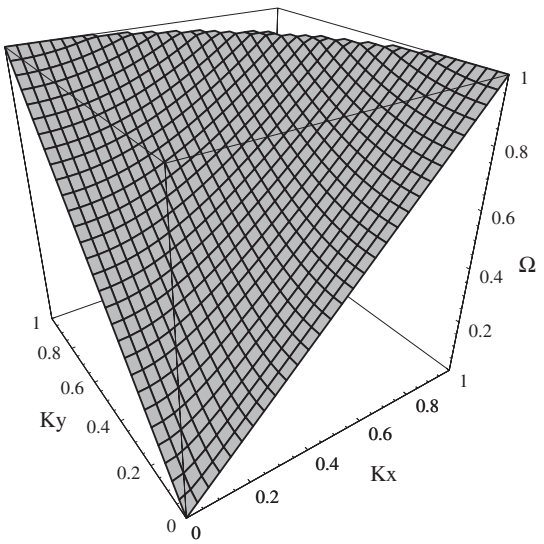

Figure 1. Analytical two-dimensional dispersion surface.

with $T \to 0$, the magnitude of the analytical dispersion relationship may be expressed as

$$\Omega = \left(\frac{L}{\Delta x}\right)\left(K_x^2 + \left(\frac{\Delta x}{\Delta y}\right)^2 K_y^2\right)^{1/2} \tag{13}$$

For $L = \Delta x = \Delta y$ the expression is simply

$$\Omega = \sqrt{K_x^2 + K_y^2} \tag{14}$$

The two-dimensional surface described by the above relationship is shown in Figure 1. Note that the continuum relationship is monotonic everywhere with a linear slope of unity. The curve obtained from a slice through the two-dimensional surface is identical to the curve obtained by one-dimensional analysis when the dependent variable is defined as $K \equiv \sqrt{K_x^2 + K_y^2}$. The dispersion surfaces for the discrete schemes will all be compared to this surface.

3. DISCRETIZATION

The finite element approximations are implemented by first establishing a weighted residual statement for the governing equations. Using

$$\langle a, b \rangle \equiv \int_\Omega ab \, \mathrm{d}x \tag{15}$$

and the approximations

$$\zeta(x, y) \simeq \sum_{k=1}^{n} \zeta_k \phi_k(x, y) \tag{16}$$

$$u(x, y) \simeq \sum_{k=1}^{n} u_k \phi_k(x, y) \tag{17}$$

$$v(x, y) \simeq \sum_{k=1}^{n} v_k \phi_k(x, y) \tag{18}$$

where ϕ_k are the standard linear basis functions for two-dimensional triangular elements, the weighted residual statements for the continuity and momentum equations are

$$(\hat{\mathrm{i}}\omega)\langle\psi_j, \phi_k\rangle\zeta_k + h\left\langle\psi_j, \frac{\partial\phi_k}{\partial x}\right\rangle u_k + h\left\langle\psi_j, \frac{\partial\phi_k}{\partial y}\right\rangle v_k = 0 \tag{19}$$

$$(\hat{\mathrm{i}}\omega + \tau)\langle\phi_j, \phi_k\rangle u_k + g\left\langle\phi_j, \frac{\partial\phi_k}{\partial x}\right\rangle \zeta_k = 0 \tag{20}$$

$$(\hat{\mathrm{i}}\omega + \tau)\langle\phi_j, \phi_k\rangle v_k + g\left\langle\phi_j, \frac{\partial\phi_k}{\partial y}\right\rangle \zeta_k = 0 \tag{21}$$

The weighting function, ψ_j, that appears in the continuity weighted residual statement may or may not be the same as the basis functions ϕ_j. When the matrices indicated above are populated by performing the integrations for each element, and the elemental contributions are assembled, the result is a system of algebraic equations for the unknown nodal values.

3.1. Grid configurations

The structure of the discrete equations will depend upon the connectivity and arrangement of a two-dimensional assembly of elements, thus a study of dispersion relationships must take into account the grid geometry. Consequently, discrete equations are derived and investigated for each of the patches of finite elements illustrated in Figure 2. The '6eq' patch is an assembly of six equilateral triangles, the '6b' patch is an assembly of six isosceles triangles obtained by bisecting squares, and the '4/8' patch is a collection of four '4' subpatches and one '8' subpatch of isosceles triangles. The '4' and '8' patches will always exist together and it is necessary to consider the ensemble behaviour rather than the behaviour of the subpatches separately. The '6eq' and '6b' patches can exist independently. It is assumed that these grid patches represent a typical node on the interior of an infinite and uniform computational mesh which is composed only of repeating one of the above patches. Boundary effects and boundary conditions are not considered here. For each of the element patches, the integrated elemental equations are assembled, and the equations for the centre node in each of the configurations are extracted from the global matrix system. Since the co-ordinates and nodal connectivity are different for each of the element configurations shown, the assembly procedure yields

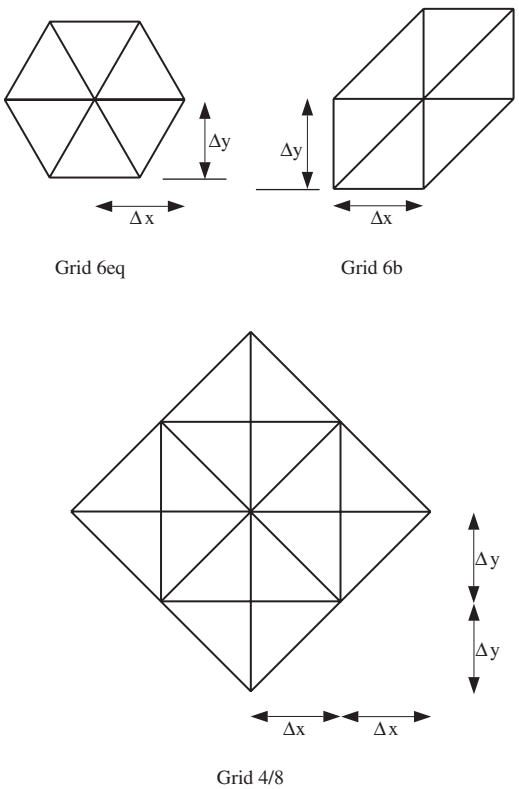

Figure 2. The patches of elements used to derive the discrete equations.

a different set of discrete equations in each case. The dispersion analysis is applied to the discrete equations obtained for each grid configuration.

An important consideration that arises during dispersion studies is the identification of the resolvable limit. For any discretization of the spatial continuum, the smallest wave is twice the node spacing. In one dimension, this is clearly the $2\Delta x$ wave, but in two dimensions this smallest resolveable wave is more ambiguous. The resolvable wavelength that can be supported by these grid patches varies slightly with configuration and wave direction. Consider a wave propagating through each of the grid patches in the x-direction. Since there are nodes lined up along the x-axis, the smallest wave is obviously $2\Delta x$. For the '6b' and '4/8' patches, the smallest resolvable wave in the y-direction is the same as the x-direction because $\Delta x = \Delta y$. However, patch '6eq' will admit a shorter wave in the y-direction than it does in the x-direction because $\Delta y = \frac{\sqrt{3}}{2}\Delta x$. For the general case of a wave travelling with components in both directions, a directional angle may be introduced as in Figure 3. For the '6b' and '4/8' patches, the smallest resolvable wave for a wave travelling at $\theta = 45^\circ$ is $2\sqrt{2}\Delta x$ based on nodal spacing in the 45° direction. The smallest wave that can propagate at $\theta = 60^\circ$ through the '6eq' grid is $2\Delta x$ because all the edges of the triangles are equal length. For waves travelling in other directions, identifying the smallest resolvable wave is less clear. It is desired to scale

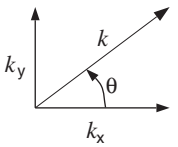

Figure 3. Definition of θ for describing the direction of wave propagation.

the wave numbers according to their resolvable limit such that the smallest wave corresponds to the non-dimensional wave number equal to unity. In the following analysis, the k_x and k_y wave number components will be scaled with the corresponding grid spacing Δx or Δy. The non-dimensional frequency in Equation (9) is scaled with a length scale, L, which characterizes the resolvable limit of the grid patch. For patch '6b' and patch '4/8' $L = \Delta x = \Delta y$ and for patch '6eq' $L = \Delta x = \frac{2}{\sqrt{3}}\Delta y$.

3.2. *Primitive equation scheme*

In the following discussion, the primitive scheme will be defined as the use of linear, equal order triangular finite element interpolation to discretize the primitive form of the governing equations as expressed in Equations (1)–(3). The weighting function in Equation (19) is chosen such that $\psi_j = \phi_j$.

After the Fourier modes are substituted into the discrete equations for the '6eq' patch of elements, setting the determinant of the system matrix for the Fourier amplitudes equal to zero yields

$$(\hat{\imath}\omega + \tau)\left(-\omega^2 + (\hat{\imath}\tau)\omega + \frac{gh}{\beta_1^2}\left[\left(\frac{2\alpha_1}{\Delta x}\right)^2 + \left(\frac{3\alpha_2}{\Delta y}\right)^2\right]\right) = 0 \tag{22}$$

where

$$\begin{aligned}
\beta_1 &= \cos(k_x\Delta x) + \cos(k_x\Delta x/2 + k_y\Delta y) + \cos(k_x\Delta x/2 - k_y\Delta y) + 3 \\
\alpha_1 &= 2\sin(k_x\Delta x) + \sin(k_x\Delta x/2 + k_y\Delta y) + \sin(k_x\Delta x/2 - k_y\Delta y) \\
\alpha_2 &= \sin(k_x\Delta x/2 + k_y\Delta y) - \sin(k_x\Delta x/2 - k_y\Delta y)
\end{aligned} \tag{23}$$

The corresponding roots are the numerical artefact

$$\omega = \hat{\imath}\tau \tag{24}$$

and the roots

$$\omega_{p6\text{eq}} = \left(\frac{\hat{\imath}\tau}{2}\right) \pm \left(\frac{gh}{\beta_1^2}\left[\left(\frac{2\alpha_1}{\Delta x}\right)^2 + \left(\frac{3\alpha_2}{\Delta y}\right)^2\right] - \left(\frac{\tau}{2}\right)^2\right)^{1/2} \tag{25}$$

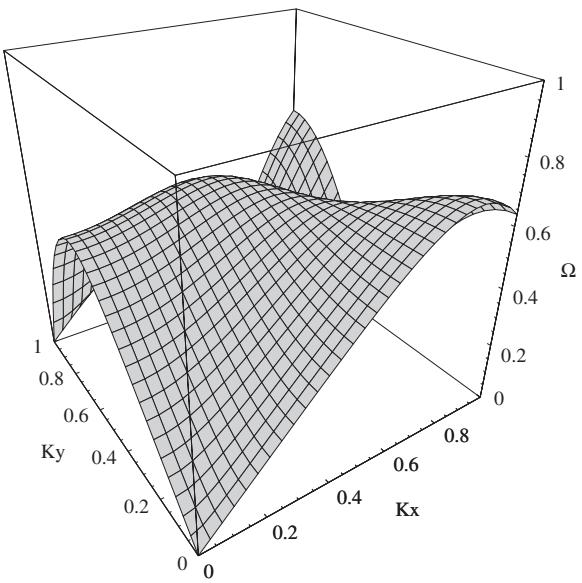

Figure 4. Dispersion surface for the primitive equation scheme on grid patch '6eq', view 1.

For plotting the surfaces described by Equation (25), the equation is cast into non-dimensional form using the non-dimensional variables presented in Equations (9)–(12). When $T \to 0$, the non-dimensional dispersion relationship for the primitive scheme on grid '6eq' is

$$\Omega_{p6\mathrm{eq}} = \frac{2}{\pi\beta_1}\sqrt{\alpha_1^2 + 3\alpha_2^2} \tag{26}$$

When $T \neq 0$, there is a small bifurcation near the resolvable limit but the gross properties of the dispersion surface remain unaffected. For typical friction values, T is small and there is no loss of utility in examining the dispersion surface for $T \to 0$.

Two views of the non-dimensional dispersion surface for configuration '6eq' are presented in Figures 4 and 5. Observe that the surface folds completely along the K_y axis but not along the K_x axis. Additionally, some folding of the surface occurs for values of $0° < \theta < 90°$, but the surface does not descend all the way to zero within the resolvable limit anywhere except along the K_y axis ($\theta = 90°$). Note that all waves for which

$$\sqrt{K_x^2 + K_y^2} > 1 \tag{27}$$

are unresolved and do not exist in the discrete realm. This includes the upturned 'fan' that appear in the figures for large wave numbers. The dispersion surface presented here differs from the result presented by Foreman [11] in the existence of a complete fold. The difference is due to the use here of separate scaling for the x and y wave numbers. It will be shown later that this is the appropriate scaling.

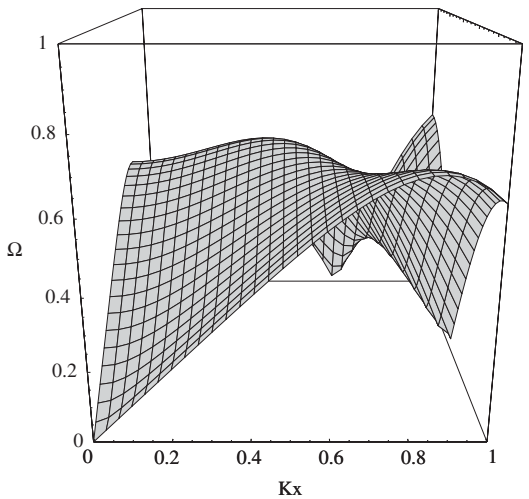

Figure 5. Dispersion surface for the primitive equation scheme on grid patch '6eq', view 2.

For the '6b' patch of elements, setting the determinant of the system matrix for the Fourier amplitudes equal to zero gives

$$(\hat{\imath}\omega + \tau)\left(-\omega^2 + (\hat{\imath}\tau)\omega + \frac{4gh}{\beta_1^2}\left[\left(\frac{\alpha_1}{\Delta x}\right)^2 + \left(\frac{\alpha_2}{\Delta y}\right)^2\right]\right) = 0 \tag{28}$$

but with new definitions

$$\begin{aligned}
\beta_1 &= \cos(k_x\Delta x) + \cos(k_y\Delta y) + \cos(k_x\Delta x + k_y\Delta y) + 3 \\
\alpha_1 &= 2\sin(k_x\Delta x) - \sin(k_y\Delta y) + \sin(k_x\Delta x + k_y\Delta y) \\
\alpha_2 &= -\sin(k_x\Delta x) + 2\sin(k_y\Delta y) + \sin(k_x\Delta x + k_y\Delta y)
\end{aligned} \tag{29}$$

The root

$$\omega = \hat{\imath}\tau \tag{30}$$

is a numerical artefact and the remaining two roots are

$$\omega_{p6b} = \left(\frac{\hat{\imath}\tau}{2}\right) \pm \left(\frac{4gh}{\beta_1^2}\left[\left(\frac{\alpha_1}{\Delta x}\right)^2 + \left(\frac{\alpha_2}{\Delta y}\right)^2\right] - \left(\frac{\tau}{2}\right)^2\right)^{1/2} \tag{31}$$

Non-dimensionalizing as before, the dispersion surface for the '6b' configuration is presented in Figure 6 for $T \to 0$. Unlike the result for configuration '6eq', the dispersion relationship for the '6b' configuration has two identical, full folds along the K_x and K_y axes. Again note that all waves for which

$$\sqrt{K_x^2 + K_y^2} > 1 \tag{32}$$

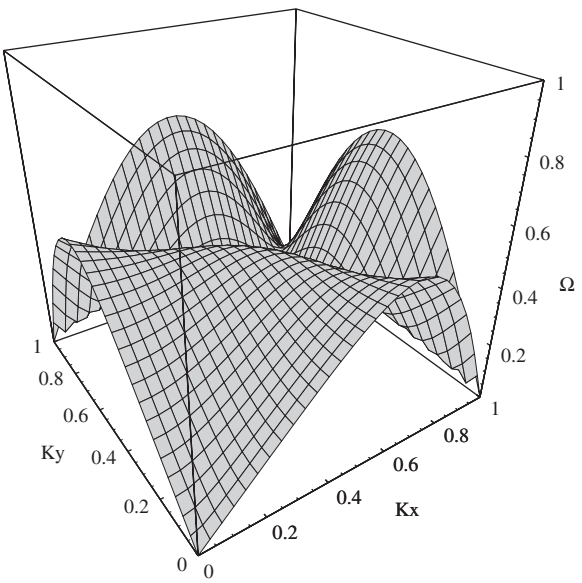

Figure 6. Dispersion surface for the primitive equation scheme on grid patch '6b'.

are unresolved and do not exist in the discrete realm. This includes the upturned 'fans' that appear in the figures for large wave numbers.

The '4/8' patch is more complicated to analyse. Note that there are two types of nodes that exist in the '4/8' patch in Figure 2, nodes connected to four other nodes and nodes connected to eight other nodes. Performing separate analyses on the overlapping stencils does not necessarily permit conclusions about the behaviour of the ensemble. Rather, an ensemble analysis must be performed and the stencils of four element patches are substituted into the equation for the eight element stencil to eliminate the nodal unknowns for the four sub-patches. This condensed set of discrete equations is analysed similar to the previous grid configurations; however, there is a complication since the resulting dispersion relationship is a sixth-order polynomial and the roots must be obtained numerically. The dispersion relationship is

$$\sum_{j=1}^{7} a_j \omega^{(j-1)} = 0 \tag{33}$$

where the expressions for the a_j coefficients may be found in Reference [15]. The magnitude of the physical roots for the '4/8' configuration are plotted in Figure 7 along the K_x axis ($\theta = 0°$) and the K_y axis ($\theta = 90°$) together with the widely published one-dimensional dispersion curve for $T \to 0$. It may be observed that these slices of the '4/8' surface are identical to the one-dimensional result. Figure 7 also shows two slices through the '6eq' and '6b' dispersion surfaces for $\theta = 0°$ and 90°. The slices of the dispersion surface for patch '6b', like the '4/8' case, are identical to the one-dimensional result. The $\theta = 90°$ slice of the '6eq' grid is also identical to the one-dimensional result, but the $\theta = 0°$ slice is different. This later case corresponds to a wave propagating only in the x-direction and it may be observed both from inspection of the two-dimensonal surface and from the one-dimensional slice that the '6eq'

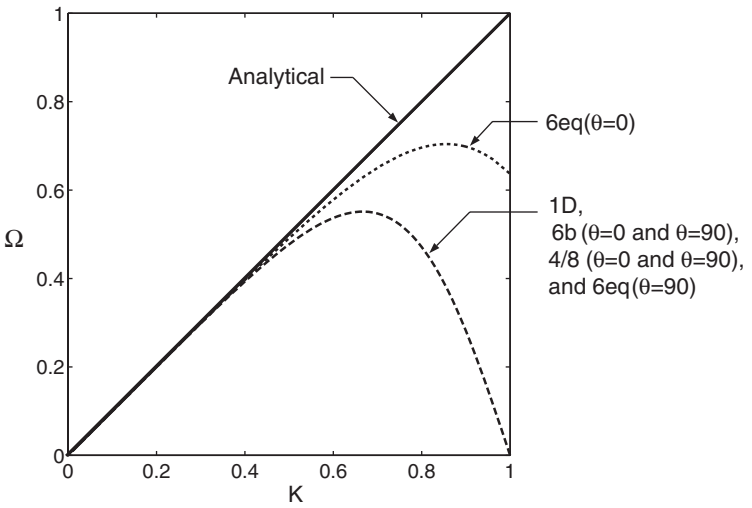

Figure 7. Comparison of the one-dimensional primitive dispersion curve and slices of the two-dimensional primitive dispersion surface for configuration '6eq', '6b' and '4/8' are shown in the analytical result. $K = \sqrt{K_x^2 + K_y^2}$.

dispersion relationship does not fold all the way back to zero. Therefore, while the '4/8' and '6b' configuration dispersion results along the x- and y-direction are identical to the one-dimensional result, the two-dimensional result for patch '6eq' in the x-direction contradicts the one-dimensional result.

All of the dispersion surfaces are asymptotic to the continuum dispersion surface for low wave numbers. This means that all of the discretizations accurately represent long waves as is necessary for a scheme to be convergent. However, practical use of these configurations will result in some of the wave content being along one of the folded directions. Therefore, we can anticipate that these discretizations will yield oscillatory results. Since the dispersion surface for grid configuration '6eq' folds completely in only one direction, at $\theta = 90°$, and not for $\theta = 0°$, smoother results may be possible when using a grid based upon configuration '6eq'. Consequently, depending on the wave propagation direction, the solution may reside mostly in the monotonic dispersion region. We emphasize that *this difference in dispersion behaviour is due to grid configuration and wave propagation direction and not due to the choice of linear finite element interpolation*. It has long been known that superior results could be obtained on a grid composed of equilateral triangles such as those in configuration '6eq'. The incomplete folding of the dispersion surface may be responsible for this behaviour.

An explanation of the different '6eq' behaviour along the $\theta = 0°$ and 90° directions is that the discrete stencil is subtly different between one and two dimensions for the '6eq' patch. It is illustrative to simplify the two-dimensional discrete equations by assuming one-dimensional flow and to consider how the simplified two-dimensional equations compare to the one-dimensional discrete equations. Refering to the node numbers in Figure 8, the discrete

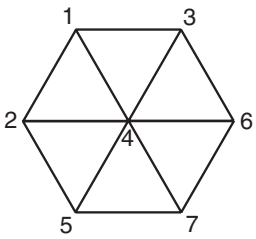

Figure 8. Node numbers for patch '6eq'.

continuity equation for the centre node (node 4) is

$$(\hat{\mathrm{i}}\omega)(\zeta_1+\zeta_2+\zeta_3+6\zeta_4+\zeta_5+\zeta_6+\zeta_7)$$
$$+\frac{2h}{\Delta x}(u_3-u_1+2(u_6-u_2)+u_7-u_1)+\frac{3h}{\Delta y}(v_1-v_5+v_3-v_7)=0 \tag{34}$$

For a wave travelling through the patch in the x-direction with no flow component in the y-direction,

$$\frac{\partial}{\partial y}=0 \tag{35}$$

all $v_j=0$, and

$$\zeta_1=\zeta_5, \quad \zeta_3=\zeta_7 \tag{36}$$

$$u_1=u_5, \quad u_3=u_7 \tag{37}$$

With these simplifications, the discrete equation (34) reduces to

$$(\hat{\mathrm{i}}\omega)(2\zeta_1+\zeta_2+2\zeta_3+6\zeta_4+\zeta_6)+\frac{4h}{\Delta x}(u_3-u_1+u_6-u_2)=0 \tag{38}$$

or to compare to a one-dimensional stencil the above may be written with $\pm j$ notation as

$$\frac{(\hat{\mathrm{i}}\omega)}{12}(\zeta_{j-1}+2\zeta_{j-1/2}+6\zeta_j+2\zeta_{j+1/2}+\zeta_{j+1})+\frac{h}{3\Delta x}(u_{j+1/2}-u_{j-1/2}+u_{j+1}-u_{j-1})=0 \tag{39}$$

This is *not* the same as the following standard one-dimensional linear Galerkin interpolation stencil

$$\frac{(\hat{\mathrm{i}}\omega)}{6}(\zeta_{j-1}+4\zeta_j+\zeta_{j+1})+\frac{h}{2\Delta x}(u_{j+1}-u_{j-1})=0 \tag{40}$$

Now consider a wave travelling in the y-direction only, then

$$\frac{\partial}{\partial x}=0 \tag{41}$$

all $u_j = 0$, and

$$\zeta_1 = \zeta_3, \quad \zeta_5 = \zeta_7 \tag{42}$$

$$v_1 = v_3, \quad v_5 = v_7, \quad v_6 = v_2 = v_4 \tag{43}$$

With these simplifications, the discrete equation (34) reduces to

$$(\hat{\imath}\omega)(2\zeta_1 + 8\zeta_4 + 2\zeta_5) + \frac{6h}{\Delta y}(v_1 - v_5) = 0 \tag{44}$$

This *is* equivalent to the one-dimensional stencil in Equation (40). The same result is found when the 2D to 1D reductions are made to the terms in the discrete momentum equations because the momentum equations contain the same stencils as the continuity equation. Furthermore, the continuity and momentum stencils for the '4/8' and '6b' patches simplify exactly to the one-dimensional stencil for both x and y directions.

Observe that the simplification for an x-direction wave on the '6eq' grid suggests a staggered grid effect and the dispersion relation is non-folded in that direction. It can be shown that staggered grid schemes generate a $\sin(k\,\Delta x/2)$ term in the dispersion relationship which moves the folded portion of the dispersion curve beyond the resolvable limit, resulting in smooth solutions. This effect may be demonstrated by plotting the equations further along the x-axis and observing that they will fold back to zero at twice the resolvable limit. There is a similar $\sin(k\Delta x/2)$ term that appears in the x-direction '6eq' linear finite element dispersion relationships. None of the other grid configurations considered here provide a mechanism for producing this term.

3.3. Wave equation formulation

In this section, the generalized wave continuity equation scheme (GWCE) [5] is considered. The GWCE is obtained when the continuity Equation (1) is combined with the momentum Equations (2) and (3) and is reformulated as

$$(\hat{\imath}\omega)(\hat{\imath}\omega + G)\zeta + (G - \tau)h\left(\frac{\partial u}{\partial x} + \frac{\partial v}{\partial y}\right) - gh\left(\frac{\partial^2 \zeta}{\partial x^2} + \frac{\partial^2 \zeta}{\partial y^2}\right) = 0 \tag{45}$$

The GWCE is used in place of the continuity equation and is solved in conjunction with the momentum equations. It has been shown that the same solutions will be admitted by solving either 1 or 45 provided that the initial condition satisfies Equation (1) [10].

The discrete equations are derived for the centre node in the grid patches '6eq', '6b' and '4/8' and Fourier expansions are substituted into the discrete stencils as described previously. The dispersion relationship is obtained when the determinant of Fourier system matrix is set equal to zero. For the '6eq', the result is

$$(\hat{\imath}\omega + \tau)\beta_1\left((\hat{\imath}\omega + \tau)\beta_1\left[(-\omega^2 + \hat{\imath}G\omega)\beta_1 + gh\left(\frac{12}{\Delta x^2}\beta_2 + \frac{3}{\Delta y^2}\beta_3\right)\right]\right.$$
$$\left. + (G - \tau)gh\left[\left(\frac{2\alpha_1}{\Delta x}\right)^2 + \left(\frac{3\alpha_1}{\Delta y}\right)^2\right]\right) = 0 \tag{46}$$

where

$$\begin{aligned}
\beta_1 &= \cos(k_x\Delta x) + \cos(k_x\Delta x/2 + k_y\Delta y) + \cos(k_x\Delta x/2 - k_y\Delta y) + 3\\
\beta_2 &= 1 - \cos(k_x\Delta x)\\
\beta_3 &= 3 - 2\cos(k_x\Delta x/2 + k_y\Delta y) - 2\cos(k_x\Delta x/2 - k_y\Delta y) + \cos(k_x\Delta x)\\
\alpha_1 &= 2\sin(k_x\Delta x) + \sin(k_x\Delta x/2 + k_y\Delta y) + \sin(k_x\Delta x/2 - k_y\Delta y)\\
\alpha_2 &= \sin(k_x\Delta x/2 + k_y\Delta y) - \sin(k_x\Delta x/2 - k_y\Delta y)
\end{aligned} \tag{47}$$

One of the roots is

$$\omega = \hat{\imath}\tau \tag{48}$$

which leaves a cubic expression for the other three roots of ω.

Kolar *et al.* [16] recommend setting $G \geqslant \tau$ to optimize mass conserving and folding properties. When $G = \tau$ the coefficient matrix changes slightly with the result being

$$(\hat{\imath}\omega + \tau)\beta_1\left((\hat{\imath}\omega + \tau)\beta_1\left[(-\omega^2 + \hat{\imath}\tau\omega)\beta_1 + gh\left(\frac{12}{\Delta x^2}\beta_2 + \frac{3}{\Delta y^2}\beta_3\right)\right]\right) = 0 \tag{49}$$

which leaves a duplicate root

$$\omega = \hat{\imath}\tau \tag{50}$$

and leaves a quadratic expression for the other two roots of ω,

$$\omega_{w6\mathrm{eq}} = \left(\frac{\hat{\imath}\tau}{2}\right) \pm \left(\frac{gh}{\beta_1}\left[\frac{12}{\Delta x^2}\beta_2 + \frac{3}{\Delta y^2}\beta_3\right] - \left(\frac{\tau}{2}\right)^2\right)^{1/2} \tag{51}$$

The non-dimensional surface defined by Equation (51) is presented in Figure 9 for $T \to 0$. Observe that it is monotonic for all directions.

The dispersion relationships for the GWCE scheme with $G = \tau$ on grid configuration '6b' is

$$\omega_{w6\mathrm{b}} = \left(\frac{\hat{\imath}\tau}{2}\right) \pm \left(\frac{12gh}{\beta_1}\left[\frac{\beta_2}{(\Delta x)^2} + \frac{\beta_3}{(\Delta y)^2}\right] - \left(\frac{\tau}{2}\right)^2\right)^{1/2} \tag{52}$$

where

$$\begin{aligned}
\beta_1 &= \cos(k_x\Delta x) + \cos(k_y\Delta y) + \cos(k_x\Delta x + k_y\Delta y) + 3\\
\beta_2 &= 1 - \cos(k_x\Delta x)\\
\beta_3 &= 1 - \cos(k_y\Delta y)
\end{aligned} \tag{53}$$

The non-dimensional surface is presented in Figure 10 with $T \to 0$. This surface is also monotonic for all grid configurations and all wave directions.

The dispersion surfaces in Figures 9 and 10 are typical of all the surfaces for the GWCE scheme including the '4/8' patch. Moreover, the monotonic behaviour described by the one-dimensonal relationship carries over to the two-dimensional result. In fact, a slice along the

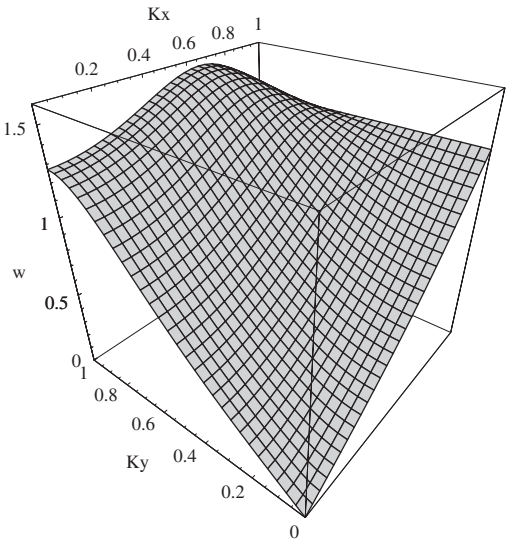

Figure 9. Dispersion surface for the GWCE scheme on grid patch '6eq'.

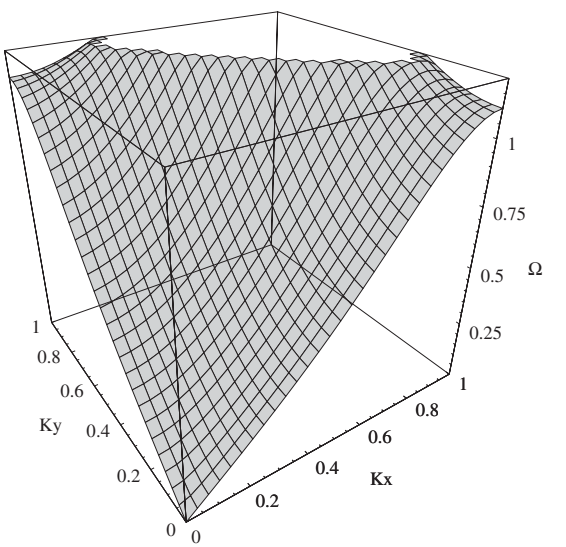

Figure 10. Dispersion surface for the GWCE scheme on grid patch '6b'.

K_x or K_y axis for patch '6b' in Figure 10 and a slice along the K_y axis for patch '6eq' is identical to the one-dimensional result. These curves are all plotted in Figure 11. However, the K_x axis slice for the '6eq' is not identical to the curve obtained from a one-dimensional derivation, but it is still monotonic.

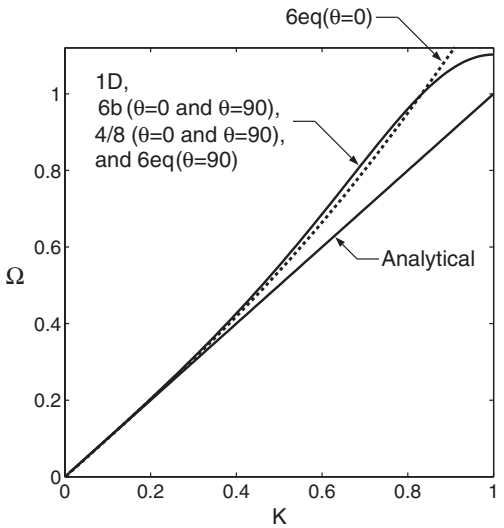

Figure 11. Comparison of the one-dimensional GWCE scheme dispersion curve and a slice of the two-dimensional GWCE dispersion surface for patch '6eq' and '6b' are shown in the analytical result.

3.4. *Cluster continuity scheme*

The cluster scheme is a new approach that we devised to overcome the mass balance problems associated with the GWCE scheme [16]. It may be thought of as an attempt to mimic a control volume scheme within a finite element framework. It is conceptually similar to the scheme presented by Giammarco and Todini [17] except that it applies to a cluster of elements instead of a control volume. The cluster scheme is obtained by modifying the weighted residual statement of the primitive scheme. The linear weighting function used to generate the weighted residual statement of the continuity equation (1) is replaced by a piecewise constant function defined on the domain composed of all the elements surrounding a node. The nodal cluster weighting function may be written as

$$\psi_j = \begin{cases} 1 & \text{in elements around node } j \\ 0 & \text{otherwise} \end{cases} \tag{54}$$

In this way, a continuity equation is generated for each node in the domain rather than elemental equations that require global assembly. This will give the numerical solution perfect mass balance globally and locally when integrated over any of these nodal subdomain clusters. This property would make it a valuable technique, which could be coupled to a transport model that similarly evaluated mass transport on nodal subdomains.

After substituting the Fourier mode into the discrete '6eq' stencil and setting the matrix determinant equal to zero, the following three roots are obtained:

$$\omega = \hat{\mathrm{i}}\tau \tag{55}$$

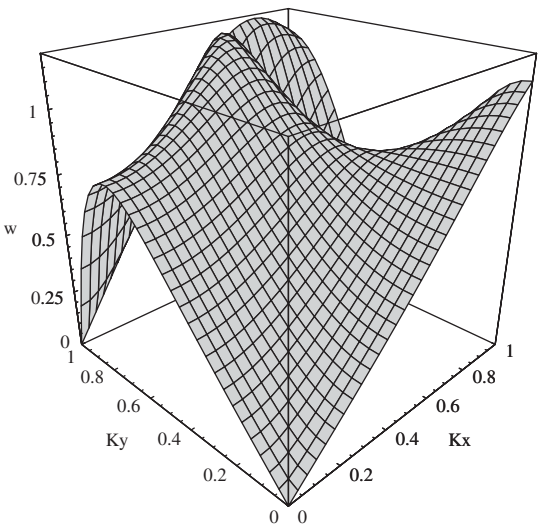

Figure 12. Dispersion surface for cluster scheme on grid patch '6eq'.

and

$$\omega_{c6\mathrm{eq}} = \left(\frac{\hat{\mathrm{i}}\tau}{2}\right) \pm \left(\frac{gh}{\beta_1\beta_2}\left[3\left(\frac{\alpha_1}{\Delta x}\right)^2 + \frac{27}{4}\left(\frac{\alpha_2}{\Delta y}\right)^2\right] - \left(\frac{\tau}{2}\right)^2\right)^{1/2} \tag{56}$$

where now

$$\beta_2 = \cos(k_x\Delta x) + \cos(k_x\Delta x/2 + k_y\Delta y) + \cos(k_x\Delta x/2 - k_y\Delta y) + \frac{3}{2} \tag{57}$$

and β_1, α_1 and α_2 are as defined in Equation (23). Non-dimensionalizing and allowing for $T \to 0$, the dispersion relationship may be expressed as

$$\Omega_{c6\mathrm{eq}} = \frac{\sqrt{3}}{\pi}\sqrt{\frac{\alpha_1^2 + 3\alpha_2^2}{\beta_1\beta_2}} \tag{58}$$

Similar expressions may be derived for all the other grid patches and non-dimensionalized as described above. The two-dimensional surface for the cluster dispersion relation for grid '6eq' is shown in Figure 12. The similarities between the cluster surfaces and the primitive surfaces may be observed. Like the primitive '6eq' dispersion result, the '6eq' dispersion for the cluster scheme is fully folded in the y-direction but is not folded in the x-direction. Compare Equation (58) to the dispersion relationship for the primitive scheme on patch '6eq' in Equation (26) and observe the great similarity between $\Omega_{c6\mathrm{eq}}$ and $\Omega_{p6\mathrm{eq.}}$ There is a slight difference in the constant in front of the radical and note that β_1 is approximately equal to $\sqrt{\beta_1\beta_2}$. This similarity exists between the cluster and primitive scheme for all the grid configurations. The cluster dispersion result for the '6b' and '4/8' grid configurations are fully folded in both the x- and y-direction. The cluster surface is steeper than the primitive surface but has the same shape as the primitive surface in each case.

While the two-dimensional dispersion analysis results for the cluster scheme are similar to those of the primitive equation scheme, they are very different from the results obtained from one-dimensional dispersion analysis. Using a one-dimensional implementation of the cluster scheme, the discrete equations are

$$\frac{(\hat{\imath}\omega)}{4}(\zeta_{j-1} + 2\,\zeta_j + \zeta_{j+1}) + \frac{h}{2\Delta x}(u_{j+1} - u_{j-1}) = 0 \tag{59}$$

and

$$\frac{(\hat{\imath}\omega + \tau)}{6}(u_{j-1} + 4\,u_j + u_{j+1}) + \frac{g}{2\Delta x}(\zeta_{j+1} - \zeta_{j-1}) = 0 \tag{60}$$

which leads to the dispersion relationship

$$\omega = \left(\frac{\hat{\imath}\tau}{2}\right) \pm \left(\frac{6gh}{\Delta x}\left[\frac{\sin^2(k\Delta x)}{(\cos(k\Delta x) + 1)(\cos(k\Delta x) + 2)}\right] - \left(\frac{\tau}{2}\right)^2\right)^{1/2} \tag{61}$$

Making use of the identity $\sin^2 = 1 - \cos^2$, a bit of manipulation shows that this is identical to the dispersion relationship for the wave equation scheme in one dimension

$$\omega = \left(\frac{\hat{\imath}\tau}{2}\right) \pm \left(\frac{6\,gh}{\Delta x}\left[\frac{1 - \cos(k\,\Delta x)}{(\cos(k\,\Delta x) + 2)}\right] - \left(\frac{\tau}{2}\right)^2\right)^{1/2} \tag{62}$$

Therefore, one-dimensional dispersion analysis predicts smooth, oscillation free behaviour that is identical to the wave equation behaviour.

Unfortunately, the monotonic behaviour of the one-dimensional cluster scheme does not carry over to the two-dimensional form. Rather the two-dimensional formulation manifests the same folding dispersion behaviour as the primitive scheme with a single y-direction fold on the '6eq' configuration and the same dual folds for the '6b' and '4/8' configurations. Figure 13 illustrates this by comparing the one-dimensional result with a slice through the folded portion of the two-dimensional surface of grid patch '6b'. Figure 13 shows that the two-dimensional analysis almost entirely contradicts the results of a one-dimensional analysis.

The explanation of this behaviour is that the two-dimensional stencils are different in two ways from the one-dimensional stencils. First, as demonstrated in the previous sections, restricting attention to an x-direction wave on the '6eq' grid reveals a staggered grid type of behaviour for which the dispersion relationship does not fold in that direction. The presence of the $\frac{\Delta x}{2}$ argument in Equation (57) is a manifestation of the two-dimensional discretization and does not appear in the one-dimensional result. Second, unlike the primitive and GWCE schemes, the discrete cluster continuity equation does not reduce identically to the one-dimensional stencil for *any* orientation or grid configuration. Consider the discrete cluster equation for the nodes shown in Figure 8 which may be written

$$\frac{(\hat{\imath}\omega)}{9}(\zeta_1 + \zeta_2 + \zeta_3 + 3\,\zeta_4 + \zeta_5 + \zeta_6 + \zeta_7)$$
$$+ \frac{h}{6\Delta x}(u_3 - u_1 + 2(u_6 - u_2) + u_7 - u_1) + \frac{h}{4\Delta y}(v_1 - v_5 + v_3 - v_7) = 0 \tag{63}$$

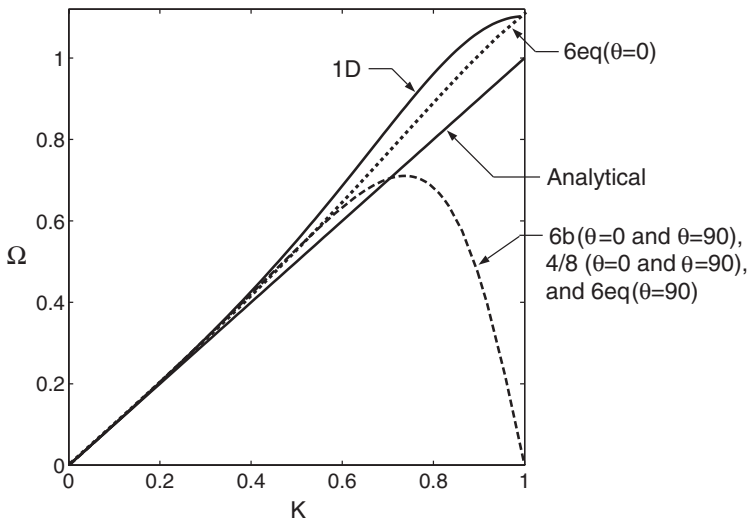

Figure 13. Comparison of the one-dimensional cluster dispersion curve and slices of the two-dimensional cluster dispersion surface for configuration '6eq', '6b' and '4/8' are shown in the analytical result.

and examining a wave propagating in only the y-direction which leads to the restrictions that

$$\frac{\partial}{\partial x} = 0 \tag{64}$$

all $u_j = 0$, and

$$\zeta_1 = \zeta_3, \quad v_1 = v_3 \tag{65}$$

$$\zeta_6 = \zeta_2 = \zeta_4 \quad v_6 = v_2 = v_4 \tag{66}$$

$$\zeta_5 = \zeta_7, \quad v_5 = v_7 \tag{67}$$

With these simplifications, the discrete equation reduces to

$$\frac{(\hat{\imath}\omega)}{9}(2\zeta_1 + 5\zeta_4 + 2\zeta_5) + \frac{h}{2\Delta y}(v_1 - v_5) = 0 \tag{68}$$

or to compare to a one-dimensional stencil equation (68) may be rearranged and written with $\pm j$ notation as

$$\frac{(\hat{\imath}\omega)}{4}\left(\frac{8}{9}\zeta_{j-1} + \frac{20}{9}\zeta_j + \frac{8}{9}\zeta_{j+1}\right) + \frac{h}{2\Delta y}(u_{j+1} - u_{j-1}) = 0 \tag{69}$$

Thus, the two-dimensional discrete cluster equations do not collapse to the one-dimensional form shown in Equation (59). This contrasts with the discrete primitive equation scheme and

the GWCE scheme which did collapse identically to a one-dimensional stencil with the same restrictions. Note that the distribution of mass for the ζ unknowns has changed from

$$1 \quad 2 \quad 1 \tag{70}$$

in Equation (59) to

$$0.8888 \quad 2.2222 \quad 0.8888 \tag{71}$$

which still sums exactly to 4 as in the one-dimensional stencil. As mentioned before, the momentum equation reduces exactly to the one-dimensional result and when Equation (69) is used in conjunction with Equation (60), the dispersion relationship is

$$\omega = \left(\frac{\hat{\imath}\tau}{2}\right) \pm \left(\frac{27\,gh}{\Delta y}\left[\frac{\sin^2(k_y \Delta y)}{(4\cos(k_y \Delta y)+5)(\cos(k_y \Delta y)+2)}\right] - \left(\frac{\tau}{2}\right)^2\right)^{1/2} \tag{72}$$

This is equivalent to the slice of the two-dimensional dispersion surface with $K_x = 0$. The only difference between the one-dimensional and two-dimensional relationships, Equation (72) and (61), is the term in the denominator that arises from the mass matrix and it is this term that causes folding in the two-dimensional implementation. This effect is not predicted by one-dimensional dispersion study. Note that the same contradiction between the one- and two-dimensional results occurs for both the x- and y-direction on grid configurations '6b' and '4/8'.

In summary, the one-dimensional analysis predicts that the cluster scheme is monotonic; however, two-dimensional analysis results are primarily folded due to a subtle change in the two-dimensional mass matrix for all grid configurations. The exception is a non-folded relationship for the x-direction on the '6eq' grid caused by the offset arrangement of nodes. This fortuitous effect is independent of the mass matrix differences. These departures from the predictions of one-dimensional analysis are significant. Moreover, simply collapsing a two-dimensional grid patch to a one-dimensional grid and checking for alignment of nodes does not reliably predict if two-dimensional behaviour will mimic the behaviour of one-dimensional equations. Even though node alignment indicates equivalence between one and two-dimensional behaviour for the primitive scheme, it does not imply the same for the cluster scheme.

4. NUMERICAL EXPERIMENTS

Numerical experiments are performed on the well-known quarter annular harbor test case [18] in order to verify the predictions of the dispersion analysis. The solutions will be found on the three computational meshes shown in Figure 14 which are represented by the patches of elements used in the analysis. Although the grid patches of Figure 2 differ slightly from the grid configurations in Figure 14, they are sufficiently similar such that the results of the analysis may be used to explain the properties of the numerical solutions. Separate simulations are performed with an M_2 wave and an M_4 wave with an amplitude of 5.0 ft (1.524 m) on the open boundary. An M_4 wave has twice the frequency of an M_2 wave which has a period of 12.42 h. The normal velocity is set to zero on the land boundary. The bathymetry varies quadratically from 10.0 ft (3.048 m) at the inner (land) boundary to 62.5 ft (19.05 m) at the outer (open)

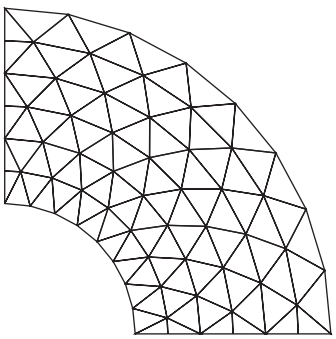

Grid 6eq

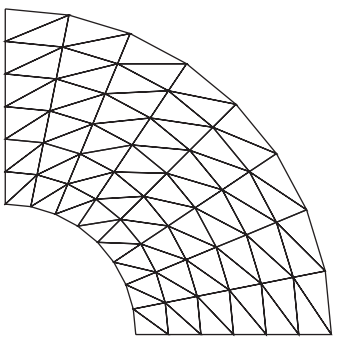

Grid 6b

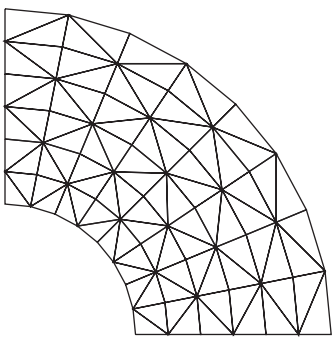

Grid 4/8

Figure 14. The three computational meshes used for numerical experiments.

boundary. A small friction value of $\tau = 0.0001$ was defined. All computations were obtained with modified versions of the ADCIRC code [19] using a time step of 5 s. The small time step was chosen such that errors in the solution were dominated by the spatial discretization. For this test case, the analytical solution is radially symmetric, so oscillations may be readily

discerned by plotting the maximum and minimum values at successive radial locations. The analytical solution has four components, sine and cosine amplitudes for elevation and for radial velocity. Values of the sine and cosine components of the Fourier decomposed elevation and velocity solutions are plotted. It is convenient to define two oscillation directions, a radial-direction and a θ-direction as suggested by defining the quarter annular domain in polar co-ordinates. The r-direction extends from the inner land boundary outward to the open boundary along radii. The θ-direction extends in the counter-clockwise direction along lines of constant r. Consider the grid configurations in Figure 14 and the idealized grid patches in Figure 2 and note that the θ-direction in the quarter annular domain corresponds to the x-direction of the patches and the r-direction corresponds to the y-direction. An oscillation in the θ-direction is indicated by the separation of the maximum and minimum values at each radial location. An oscillation in the r-direction may be discerned by the existence of an oscillatory pattern in the maximum and minimum values along the r-direction.

The numerical results for the M_2 tide using the Primitive scheme on the '6eq', '6b' and '4/8' configurations are shown in Figures 15–17. The solid line is the exact solution and the symbols represent the maximum and minimum of the computed result at each radial location. Recall that the exact solution is radially symmetric, so the noisiness of the solution is revealed by the degree to which the maximum and minimum values deviate from each other. These results are entirely consistent with the two-dimensional dispersion surfaces. As predicted, the primitive scheme on the '4/8' configuration and the '6b' configuration yielded more oscillatory solutions than the '6eq' configuration which produced minimal oscillations. The magnitude of the θ-direction wiggles are quantified as the greatest node-to-node oscillation for each of the four solution components. Figure 18 displays these magnitudes for all three grid configurations. In Figure 18 and all subsequent plots of oscillation magnitudes, the four components of the analytical solution [18] are denoted by EC for the elevation cosine component, ES for the elevation sine component, VC for the velocity cosine component, and VS for the velocity sine component. It may readily be seen that the numerical oscillations for the '6eq' grid are significantly smaller than those for the other two grid configurations. Although the '6eq' result shows negligible θ-direction wiggles, there is an observable r-direction wiggle which is consistent with the dispersion analysis result that shows a fully folded relationship in the r-direction but not in the θ-direction.

Next consider Figure 19 which displays the results for an M_4 tide using the Primitive scheme on the '6eq' configuration. Note that the r-direction wiggles are very pronounced and θ-direction wiggles have also appeared. Since an increase in forcing frequency results in greater radial oscillations, it is likely that a mechanism exists which partially suppresses the radial direction oscillations for the longer wavelength M_2 forcing. This is most likely related to boundary conditions on the inner and outer boundaries [20]. It is also clear that the r-wiggle appears due to the full folding of the dispersion surface in that direction since it is observable for the M_2 constituent. The θ-direction oscillation appears to be dependent on the existence of the larger r-direction oscillation, either due to the imperfect equilateral triangles in the test case which do not precisely line up in the x- and y-direction as in the analysis, or due to some r to θ energy transfer mechanism for the large-scale oscillations.

Figure 20 displays the results of a simulation using the cluster scheme on the '4/8' grid. The results verify the folded dispersion relationship by exhibiting the classic $2\Delta x$ oscillations. The θ-direction oscillation magnitudes for all three grid configurations are displayed graphically in Figure 21 and reveal the same trend as was seen for the primitive scheme.

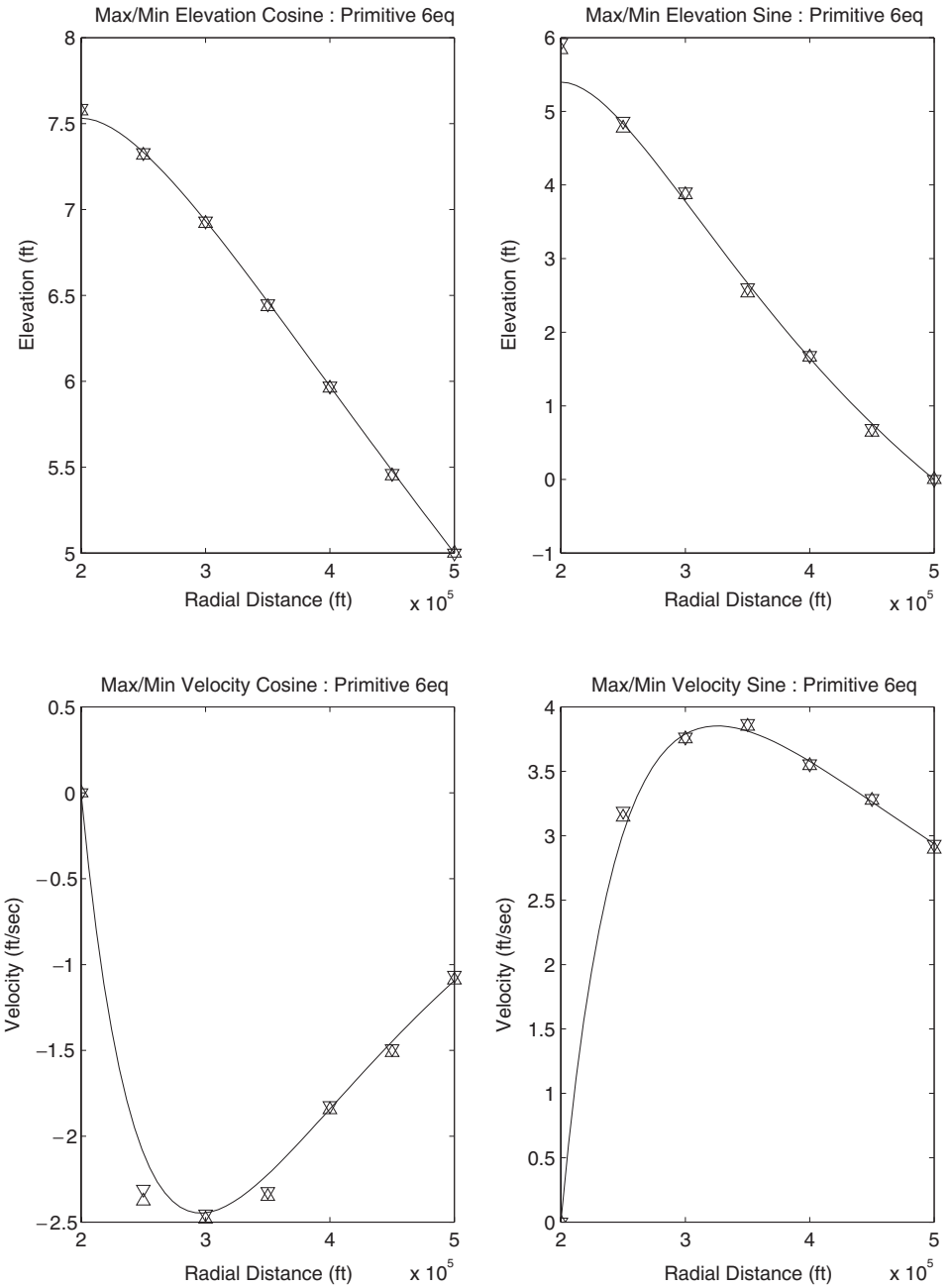

Figure 15. Results from the primitive scheme on the '6eq' grid. The solid line is the exact solution.

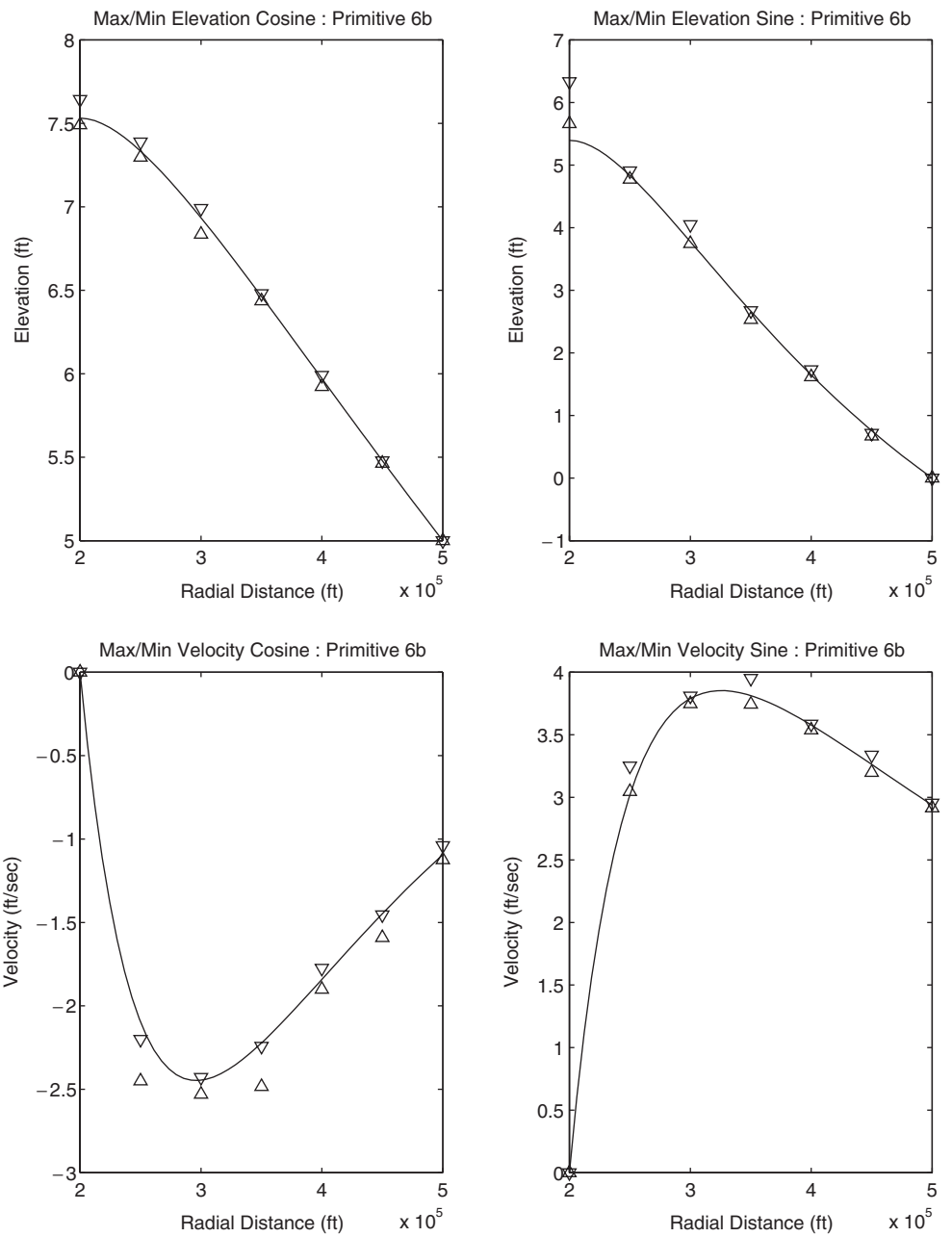

Figure 16. Results from the primitive scheme on the '6b' grid. The solid line is the exact solution.

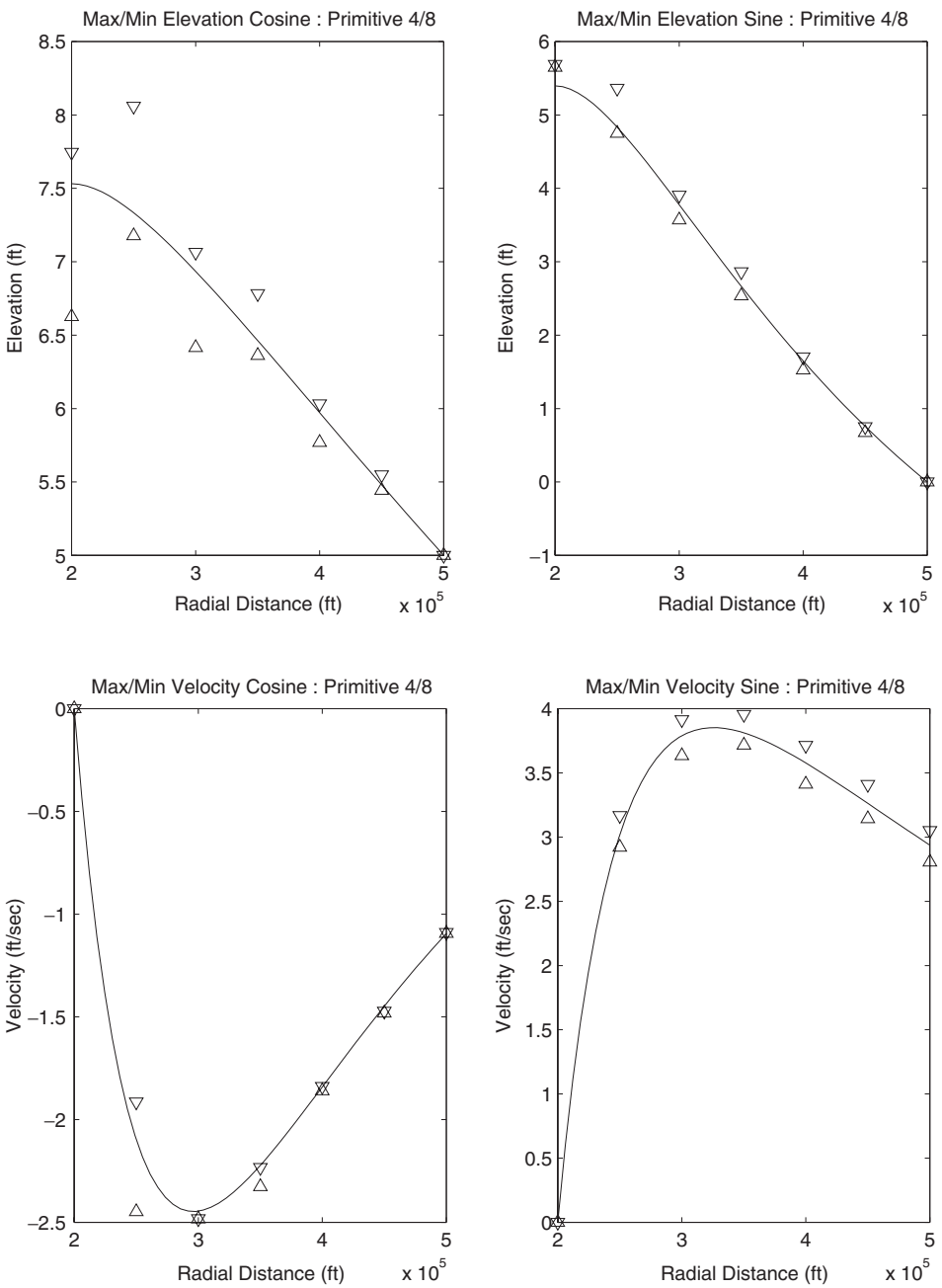

Figure 17. Results from the primitive scheme on the '4/8' grid. The solid line is the exact solution.

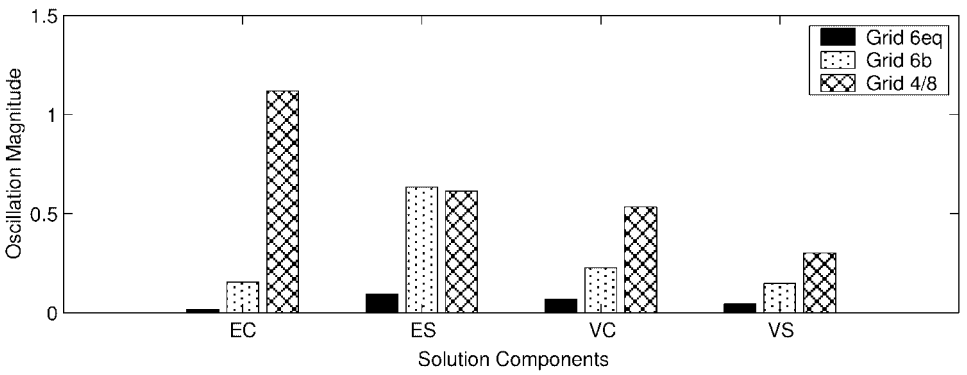

Figure 18. Maximum oscillation magnitudes for the four solution components using the primitive scheme.

Results from calculations with the GWCE scheme on grid '4/8' are shown in Figure 22. Numerical results obtained with the GWCE equation scheme on all grid configurations are consistent with the dispersion analysis and demonstrate the excellent dispersion properties of this scheme. None of the numerical solutions exhibit '$2\Delta x$' oscillations. The magnitude of maximum node-to-node θ-direction oscillations between adjacent nodes for the four solution components are shown in Figure 23 for all three grid configurations and the variability is seen to be very small for all the grid configurations. Computations with the M_4 forcing also produced minimal oscillations for all grid configurations.

5. DISCUSSION

A folded dispersion relationship serves as a proxy for the existence of spurious modes. When a dispersion relationship is folded, the existence of a second, high wave number, artificial wave is predicted. The derived dispersion relationships for all the discrete schemes are asymptotic to the analytical curve and surfaces for small wave numbers. It is the high wave number, or small wavelength, modes that have poor propagation properties.

All primitive scheme discretizations except for configuration '6eq' showed fully folded dispersion surfaces in both the x and y directions. Numerical experiments with the quarter annular test case are entirely consistent with the two-dimensional dispersion surfaces computed in this study. As predicted, the primitive equation '6b' and '4/8' configurations yield significant oscillations especially in the θ-direction while the '6eq' configuration produces only small oscillations in the r-direction with the M_2 tide. Calculations with the M_4 tide result in a much larger r-direction wiggle and the emergence of a dependent θ-direction wiggle. One-dimensional analysis of the primitive scheme suggests oscillatory solutions but it has been shown that smooth primitive solutions are possible and that dispersion properties depend upon grid configuration and wave propagation direction. Two-dimensional analysis of the primitive scheme shows that the '6b' and '4/8' configurations should be the most oscillatory since the dispersion curve is folded in both the x- and y-direction. The analysis of the '6eq' configuration reveals that the dispersion relationship is folded in the y-direction (corresponding

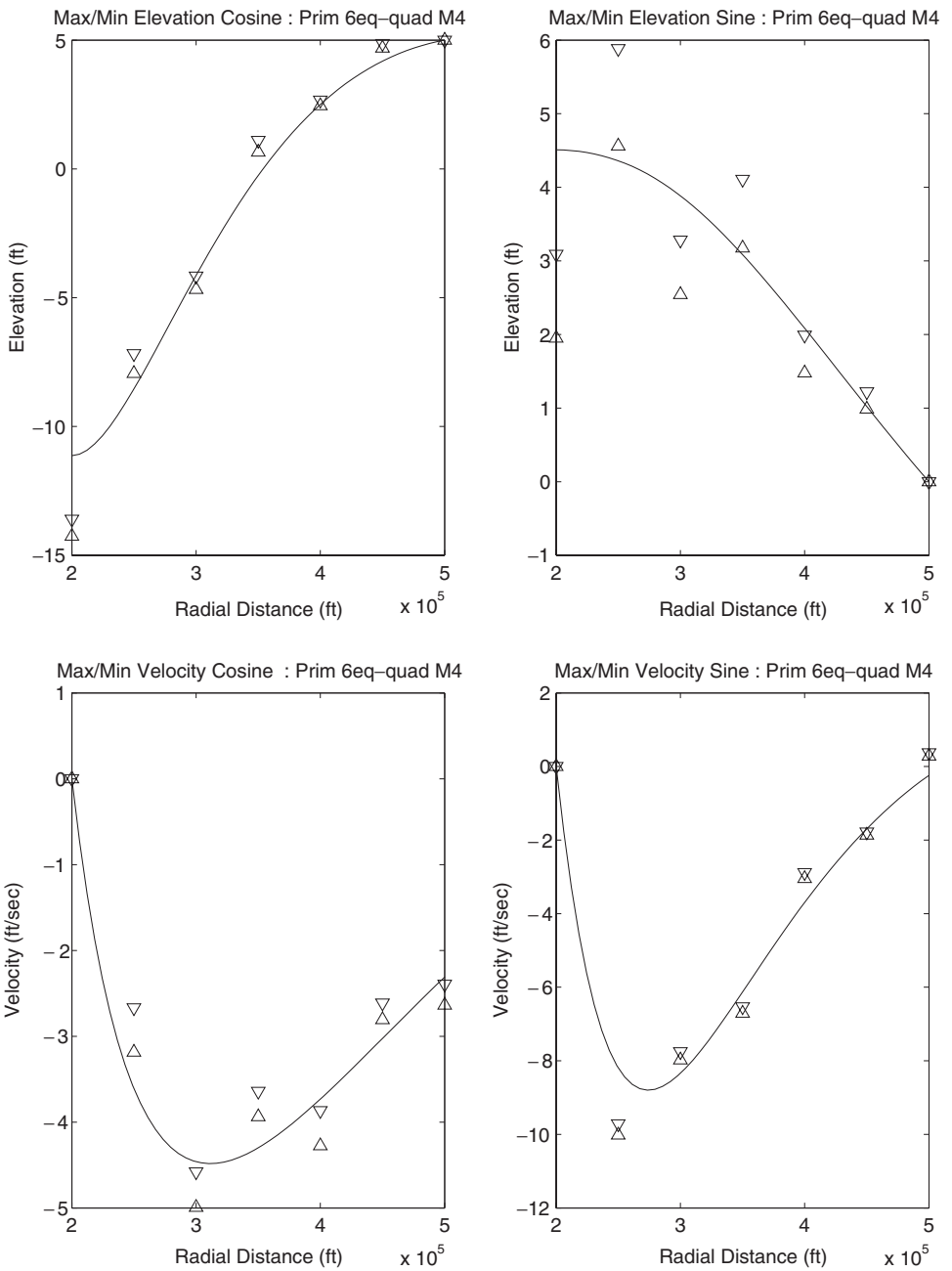

Figure 19. The M_4 results from the primitive scheme on the '6eq' grid. The solid line is the exact solution.

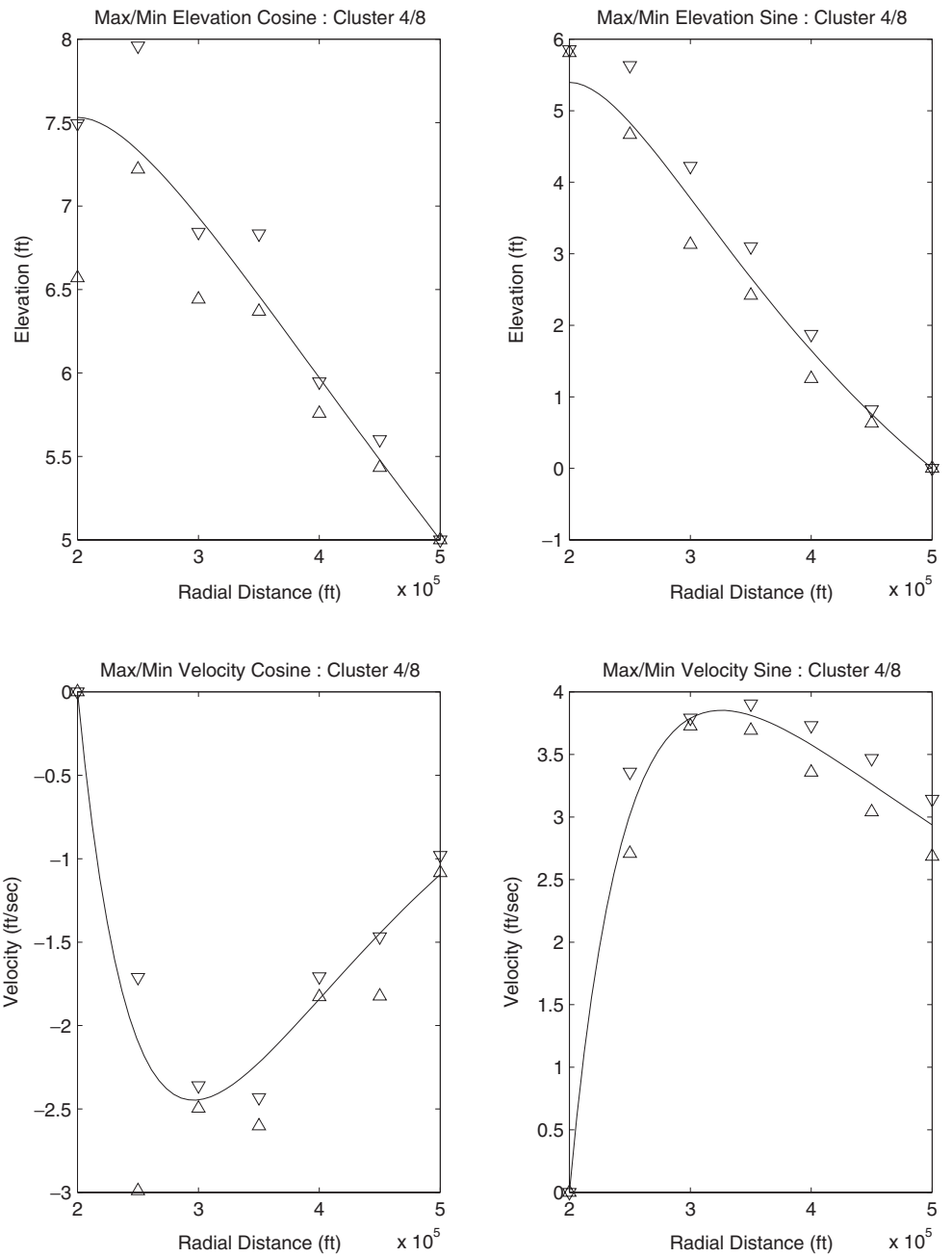

Figure 20. Results from the cluster scheme on the '4/8' grid. The solid line is the exact solution.

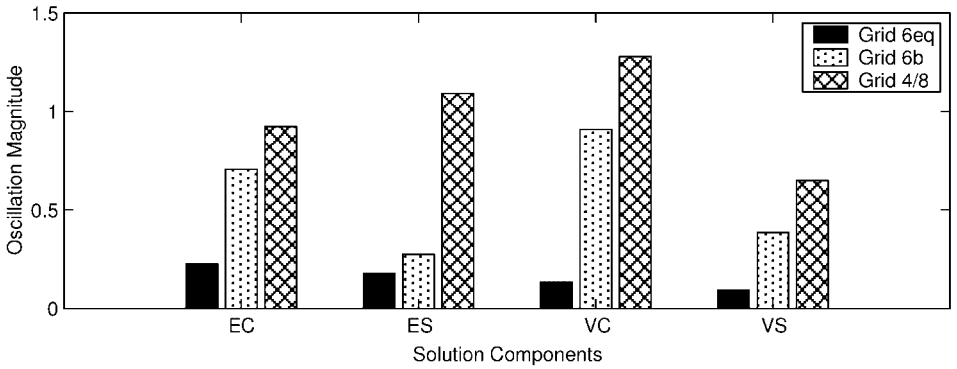

Figure 21. Maximum oscillation magnitudes for the four harmonic components using the cluster scheme.

to the r-direction) and experiments show that the oscillation occurs in this direction and that the θ-direction wiggle is small. The r-direction oscillation appears more strongly at higher frequencies, most likely because of boundary condition interaction.

Two-dimensional dispersion surfaces for the GWCE scheme are entirely monotonic for all grid configurations and in all directions. Numerical results obtained with the GWCE equation scheme on all grid configurations are consistent with the dispersion analysis and demonstrate the excellent dispersion properties of this scheme. The GWCE scheme exhibits grid and direction independent propagation behaviour, which is an ideal property.

The two-dimensional dispersion relationships for the cluster-based scheme are all qualitatively the same as the primitive equation scheme. This contradicts the one-dimensional cluster scheme dispersion analysis which predicted identical behaviour to the GWCE scheme. The numerical experiments are consistent with the two-dimensional analysis and further demonstrate the greater predictive ability of two-dimensional analysis. We note that the origins of the different behaviour for the Cluster scheme between one- and two-dimensional implementations is the structure of the mass matrix. When the two-dimensional discrete equations are allowed to collapse to a one-dimensional stencil by restricting flow to one direction, the mass matrix never collapses to the one-dimensional counterpart. Consequently, one-dimensional analysis cannot reliably predict the behaviour of a two-dimensional implementation because the structure of the two-dimensional discrete equations is somewhat different.

We note that a wave travelling at an arbitrary angle will encounter some degree of grid stagger. Consider the grid patch shown in Figure 24 and the three wave propagation directions indicated by the arrows. The figure also shows the equivalent one-dimensional grid seen by the three waves. Note that wave 'c' is supported by a grid with smaller node spacing and a staggering of nodes. This has a number of important implications.

First, superpositioning of an x- and y-directional component in a discrete solution does not add up as in the continuum solutions. The reason is that positioning and alignment of the nodes makes a critical difference in the behaviour of the solution. In general, the dispersion surfaces predict a behaviour that is different than that predicted by resolving a wave into its x and y components. If any wave could be equivalently described by the summation of an x and y wave, then the dispersion behaviour of the sum should be described by the behaviour of the components individually. But this is not suggested by the dispersion surface. Consider the

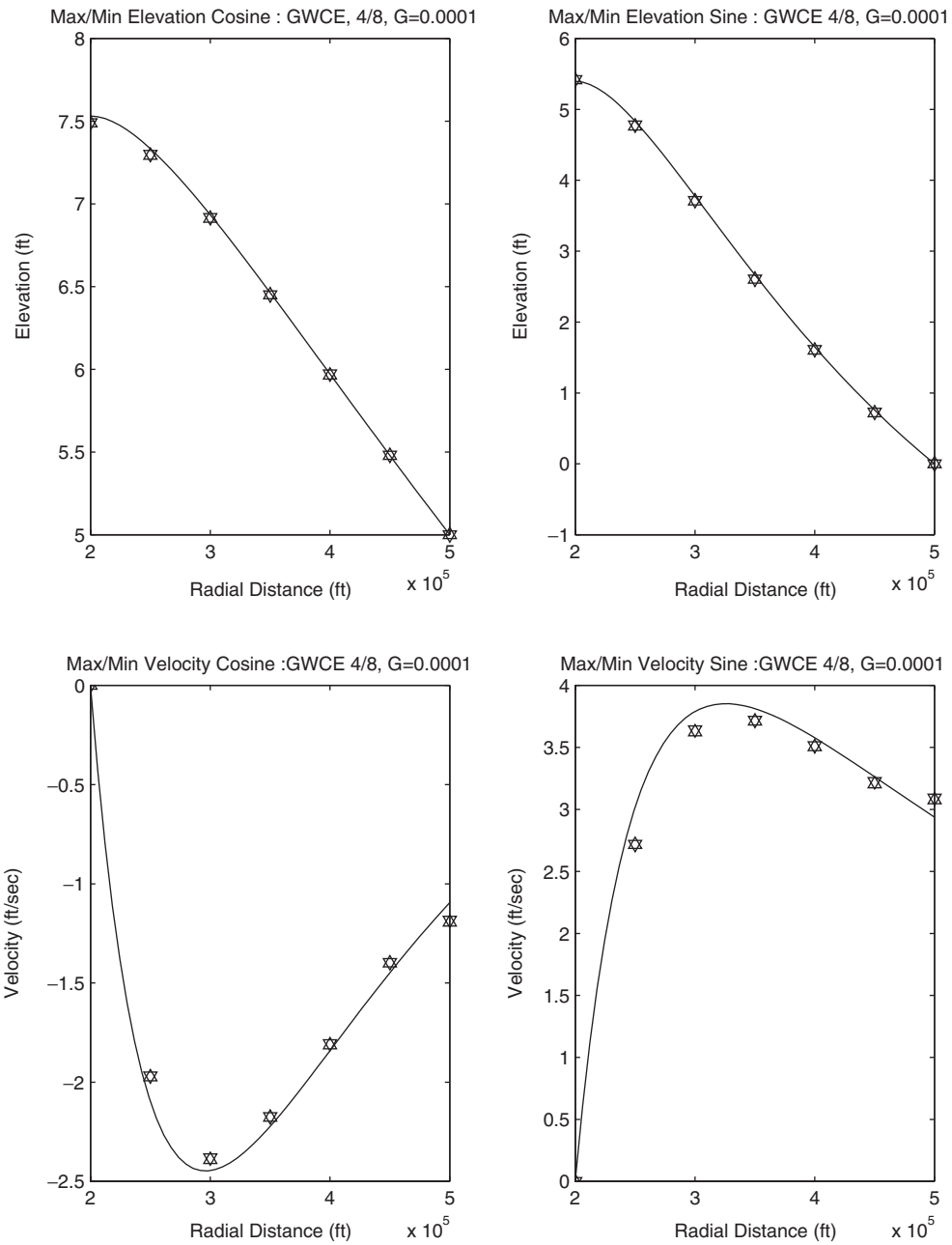

Figure 22. Results for the GWCE scheme on the '4/8' grid with $G = \tau$. The solid line is the exact solution.

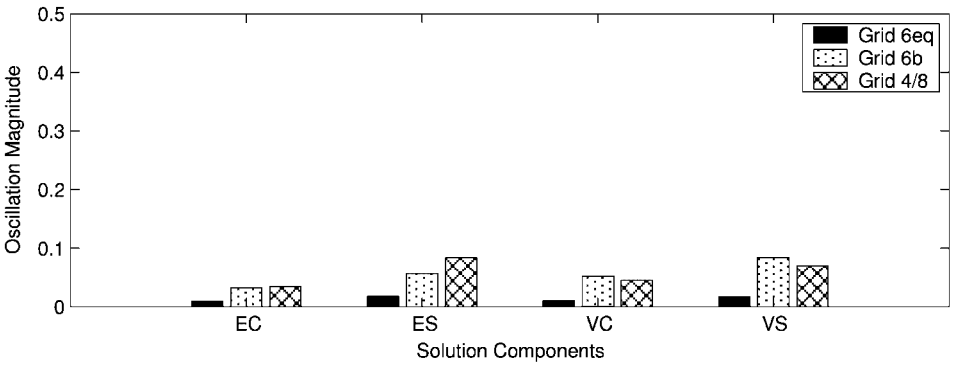

Figure 23. Maximum oscillation magnitudes for the four solution components using the GWCE scheme. Note the different vertical scale than used in Figures 18 and 21.

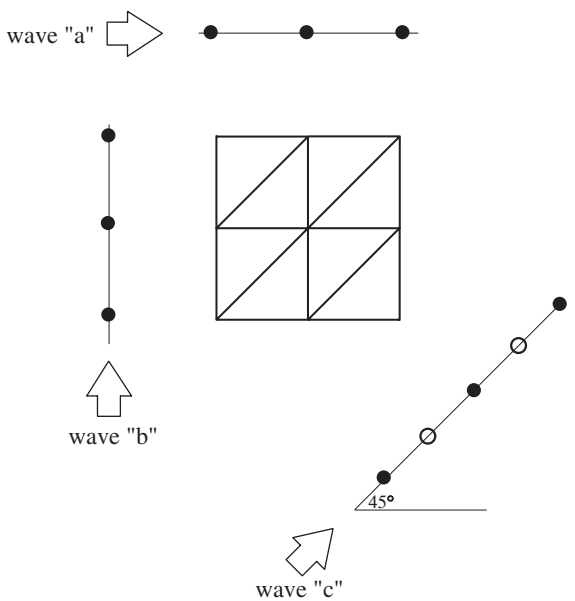

Figure 24. Effective one-dimensional grids as seen by various waves.

dispersion surface for the primitive scheme on grid '6b' as shown in Figure 6. The relationship is completely folded for both an x and y wave, but is not folded for other wave directions. A slice through the dispersion surface where $K_y = K_x/2$ is compared in Figure 25 to the slices where $K_x = 0$ and $K_y = 0$. This corresponds to a wave travelling obliquely through the grid patch at an angle $\theta = 26.6°$. Note that the slice for $\theta = 26.6°$ does not fold all the way back to zero. There is a threshold at approximately $\Omega = 0.25$ below which the behaviour is monotonic. Thus, it does appear that for an oblique wave the apparent staggering of the nodes contributes to non-folding.

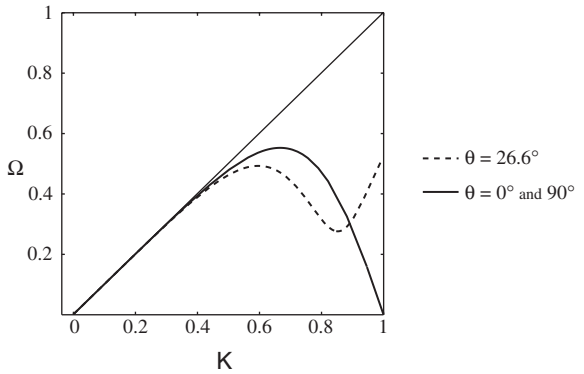

Figure 25. Comparison of several slices of the Primitive '6b' surface with $K = \sqrt{K_x^2 + K_y^2}$.

Second, for the primitive equation scheme and the cluster scheme, two-dimensional behaviour may be ascertained by examining the collapsed one-dimensional grid to check if it is effectively staggered. This has limited practical application since most real flows will contain waves propagating in many directions simultaneously. Thus, locating directions of monotonic behaviour do not guarantee non-oscillatory solutions in general. Nevertheless, such an exercise will yield insight into how a scheme behaves. An ideal scheme will have direction and grid independent dispersion behaviour such as demonstrated by the GWCE scheme.

Finally, establishing the correct resolvable limit does matter. The k_x and k_y terms are non-dimensionalized independently with the appropriate Δx and Δy measure. Use of a single measure may result in an incorrect prediction of dispersion behaviour.

6. CONCLUSIONS

Two-dimensional dispersion surfaces have been presented and have been shown to provide a more complete and accurate representation of an algorithm's numerical characteristics than can be achieved through one-dimensional analysis. For example, one-dimensional analysis of the primitive scheme predicts poor behaviour but improved results may be obtained on the two-dimensional '6eq' grid. In fact, two-dimensional analysis explains why the primitive scheme works better with equilateral triangles. Further, one-dimensional analysis of the cluster scheme predicts good behaviour but poor results are obtained in a two-dimensional implementation. Two-dimensional dispersion analysis directly contradicts the one-dimensional analysis for the cluster scheme and predicts the poor behaviour revealed by the numerical experiments.

There are several reasons that two-dimensional dispersion analysis predicts different behaviour than that suggested by one-dimensional analysis. First, a one-dimensional analysis cannot account for the effect of grid configuration which has been demonstrated to be of importance to the existence of spurious modes. Two-dimensional analysis explains the observed dependency of solution quality upon grid configuration as it relates to nodal alignment. Grid configuration is shown to affect small changes in some discrete implementations such as the primitive scheme on configuration '6eq' that result in significant modifications to the

scheme's behaviour. Second, it has been shown that subtle differences can occur in the mass matrix between a one- and two-dimensional implementation of a discrete scheme as was the case with the two-dimensional cluster scheme. Since the two-dimensional analysis is performed on the proper two-dimensional discrete equations, the influence of the mass matrix will be properly taken into account. Third, the two-dimensional dispersion behaviour for an obliquely travelling wave is different than that suggested by the sum of the x and y components for waves travelling at an angle θ. Owing to this, the properties of a numerical scheme will depend upon wave direction and one-dimensional analysis cannot illuminate this dependency. Consequently, the single numerical behaviour predicted by one-dimensional dispersion analysis is insufficient to describe the variability of a two-dimensional scheme's behaviour as it relates to grid configuration, wave propagation direction, and subtle changes that may arise from the two-dimensional implementation. These issues motivate two-dimensional dispersion analysis for evaluating spatial discretization schemes.

We recommend that new numerical solutions to the shallow water equations be subject to two-dimensional dispersion analysis for a variety of grid configurations. An ideal scheme will exhibit monotonic dispersion properties for all directions and all grid configurations.

ACKNOWLEDGEMENTS

This research was supported by the U.S. Army Engineer Research and Development Center under contract DACW 42–00–C–0006 under the Coastal Inlets Research Program with Dr Nicholas Kraus as technical leader and Dr Adele Militello as principle investigator.

REFERENCES

1. Gray WG, Lynch DR. Time stepping schemes for finite element tidal model computations. *Advances in Water Resources* 1977; **1**:83–95.
2. Walters RA, Carey GF. Analysis of spurious oscillation modes for the shallow water and Navier-Stokes equations. *Computers and Fluids* 1983; **11**:51–68.
3. Williams RT, Zienkiewicz OC. Improved finite element forms for the shallow-water wave equations. *International Journal for Numerical Methods in Fluids* 1981; **1**:81–97.
4. Laible JP, Lillys TP. A filtered solution of the primitive shallow-water equations. *Advances in Water Resources* 1997; **20**:23–35.
5. Lynch DR, Gray WG. A wave equation model for finite element tidal computations. *Computers and Fluids* 1979; **7**:207–228.
6. Platzman GW. Some response characteristics of finite element tidal models. *Journal of Computational Physics* 1981; **40**:36–63.
7. Foreman MGG. An analysis of two-step time discretizations in the solution of the linearized shallow water equations. *Journal of Computational Physics* 1983; **51**:454–483.
8. Foreman MGG. An analysis of the 'wave equation' model for finite element tidal computations. *Journal of Computational Physics* 1983; **52**:290–312.
9. Walters RA, Carey GF. Numerical noise in ocean and estuarine models. *Advances in Water Resources* 1984; **7**:15–20.
10. Kinnmark IP. *The Shallow Water Wave Equations: Formulation, Analysis and Application*. Springer Berlin, 1986.
11. Foreman MGG. A two-dimensional dispersion analysis of selected methods for solving the linearized shallow water equations. *Journal of Computational Physics* 1984; **56**:287–323.
12. Mullen R, Belytschko T. Dispersion analysis of finite element semidiscretizations of the two-dimensional wave equation. *Interanational Journal for Numerical Methods in Fluids* 1982; **18**:11–29.
13. Lynch DR, Paulsen KD. Origin of vector parasits in numerical maxwell solutions. *IEEE Transactions on Microwave Theory and Techniques* 1991; **39**(3):383–394.
14. Gray WG, Lynch DR. On the control of noise in finite element tidal computations. *Computers and Fluids* 1979; **7**:47–67.

15. Atkinson JH. Two-dimensional dispersion analysis. *Ph.D. Thesis*, University of Notre Dame, October 2002.
16. Kolar RL, Westerink JJ, Cantekin ME, Blain CA. Aspects of nonlinear simulations using shallow-water models based on the wave continuity equation. *Computers and Fluids* 1994; **23**:523–538.
17. Di Giammarco P, Todini E. A control volume finite element method for the solution of 2d overland flow problems. In *Modelling of Flood Propagation Over Initially Dry Areas*, Proceedings of the ASCE, American Society of Civil Engineers, 1994.
18. Lynch DR, Gray WG. Analytical solutions for computer flow model testing. *Journal of the Hydraulics Division* (ASCE) 1978; **104**:1409–1428.
19. Luettich RA, Westerink JJ, Scheffner NW. Adcirc, an advanced three-dimensional circulation model for shelves, coasts, and estuaries. *Technical Report*, U.S. Army Corps of Engineers, 1992.
20. Westerink JJ, Luettich RA, Wu JK, Kolar RL. The influence of normal flow boundary conditions on spurious modes in finite element solutions to the shallow water equations. *International Journal for Numerical Methods in Fluids* 1994; **18**:1021–1060.

